End versus Side Branching by Arp2/3 Complex

A. E. Carlsson,* M. A. Wear,† and J. A. Cooper†
*Department of Physics, Washington University, St. Louis, Missouri and †Department of Cell Biology and Physiology, Washington University School of Medicine, St. Louis, Missouri

ABSTRACT We investigate the issue of end versus side branching of actin filaments by Arp2/3 complex, using a combination of analytic theory, polymerization assays, and quantitative modeling. The analytic theory shows that the effect of capping protein on the initial stages of actin polymerization in the presence of Arp2/3 complex depends strongly on whether new Arp2/3 complex-induced branches grow from the sides or ends of existing filaments. Motivated by these results, we measure and quantitatively model the kinetics of actin polymerization in the presence of activated Arp2/3 complex, for a range of concentrations of capping protein. Our model includes the most important types of events involving actin and actin-binding proteins, and can be adjusted to include end branching, side branching, or both. The side-branching model gives a better fit to the experimental data than the end-branching model. An end-plus-side model including both types of branching gives a moderate improvement in the quality of the fit. Another side-branching model, based on aging of subunits' capacity for branch formation, gives a significantly better fit than the end-plus-side model. We discuss implications for actin polymerization in cells.

INTRODUCTION

Actin polymerization, which plays a crucial role in many forms of cell motility, often involves the formation of networks of actin filaments. The networks include branches between the side of one actin filament and the pointed end of another filament. Arp2/3 complex is present at the branching points, and is required for branch formation. Branched networks are seen in both ultrastructure studies of cell cytoplasm (Svitkina et al., 1997; Svitkina and Borisy, 1999) and purified proteins in vitro (Mullins et al., 1998). The role of Arp2/3 complex in stimulating actin polymerization is discussed in two recent reviews (Pollard et al., 2000; Higgs and Pollard, 2001). The branching process leads to autocatalytic polymerization (Higgs et al., 1999; Machesky et al., 1999; Pantaloni et al., 2000) in which the rate of creation of new filaments increases with the filament concentration. However, the details of the process by which new ''daughter'' filaments are generated are not well understood. Theories based on branching on filament sides and at filament barbed ends have been proposed. Structural studies of the Arp2/3 complex alone and at filament branch points (Volkmann et al., 2001; Robinson et al., 2001) support the side-branching model. In addition, fluorescence microscopy movies of filament branch formation have shown that side branching does occur, with a bias toward barbed ends in some studies (Amann and Pollard, 2001; Ichetovkin et al., 2002) or pointed ends in other studies (Fujiwara et al., 2002). On the other hand, arguments based on electron microscopy data for mother/daughter filament lengths, and the polymerization kinetics of actin in the presence of activated Arp2/3 complex, have been used to support the end-branching model (Pantaloni et al., 2000). A refinement of the side-branching model, in which the capacity of filament subunits to form new side branches ages over time, has also been proposed on the basis of fluorescence-microscopy movies (Ichetovkin et al., 2002).

Here, we discriminate among these models with experimental data from the polymerization kinetics of filament assembly in solution. The autocatalytic behavior of the Arp2/3 complex-induced branching results in a steep climb of the polymerized-actin density up to its final value. The steepness of the climb is reduced by the presence of capping protein (CP), which binds to barbed ends and thus slows polymerization. We reasoned that the strength of the CP effects should be different in end- versus side-branching models. In end-branching models, capping a filament makes it unavailable for branching, but in side-branching models the capped filament remains available, and the CP serves only to slow the growth of filaments. These differences are demonstrated in a simplified analytic model that is described below. In end-branching models, the autocatalytic growth rate goes to zero abruptly at a certain CP concentration; in side-branching models, it decreases with increasing CP concentration but never goes to zero. We have thus measured the time course of actin polymerization in the presence of Arp2/3 complex activated by GST-VCA and a range of CP concentrations, and modeled the results using both end- and side-branching models.

Simplified model for short times

At short times, the rates for growth, branching, and capping are determined by the initial concentrations of actin, Arp2/3 complex, and CP. We thus treat the polymerization kinetics via effective first-order rate constants. We also ignore pointed-end growth and capping for simplicity. Pointed ends grow slowly compared to barbed ends, and filaments

Submitted May 22, 2003, and accepted for publication August 4, 2003.

Address reprint requests to A. E. Carlsson, Dept. of Physics, Washington University, One Brookings Drive, St. Louis, MO 63130. Tel.: 314-935-5739; E-mail: aec@wuphys.wustl.edu.

0006-3495/04/02/1074/08 $2.00

nucleated by Arp2/3 complex have capped pointed ends. We thus obtain the following equations for side branching:

$$\frac{d[F]}{dt} = k_{\mathrm{br}}^{(1)}[P] - k_{\mathrm{cap}}^{(1)}[F],$$

$$\frac{d[P]}{dt} = k_{\mathrm{on}}^{(1)}[F]. \quad (1)$$

Here $[F]$ is the concentration of uncapped filaments, $[P]$ is the polymerized-actin concentration, $k_{\mathrm{br}}^{(1)}$ is the branching rate per subunit along the side of a filament, $k_{\mathrm{cap}}^{(1)}$ is the capping rate, and $k_{\mathrm{on}}^{(1)}$ is the net barbed-end monomer addition rate; all of these are assigned constant values determined by the initial protein concentrations. By transforming the expressions in Eq. 1 into a second-order equation for $[F]$, one readily shows that $[F(t)] = [F(0)]\exp(\kappa t)$, where

$$\kappa = \frac{1}{2}\left[\sqrt{k_{\mathrm{cap}}^{(1)2} + 4k_{\mathrm{on}}^{(1)}k_{\mathrm{br}}^{(1)}} - k_{\mathrm{cap}}^{(1)}\right]. \quad (2)$$

For end branching, we assume in general that filament capping excludes branching, which leads to the rate equation

$$\frac{d[F]}{dt} = (k_{\mathrm{br}}^{(1)} - k_{\mathrm{cap}}^{(1)})[F]. \quad (3)$$

For this model, $\kappa = k_{\mathrm{br}}^{(1)} - k_{\mathrm{cap}}^{(1)}$. However, for completeness we also include the case in which capping allows branching,

$$\frac{d([F] + [F^{\mathrm{B}}])}{\mathrm{dt}} = k_{\mathrm{br}}^{(1)}([F] + [F^{\mathrm{B}}]), \quad (4)$$

where $[F^{\mathrm{B}}]$ is the density of filaments capped at the barbed end. Then $\kappa = k_{\mathrm{br}}^{(1)}$, so that κ is independent of $k_{\mathrm{cap}}^{(1)}$.

Fig. 1 shows that the behavior of κ differs strongly between side- and end-branching models. Both end-branching models give straight lines, whereas the side-branching model has a gradually decaying form. These differences are sufficiently large that they should persist in more realistic models, and in measurements of polymerization kinetics. This motivates the more detailed studies described below.

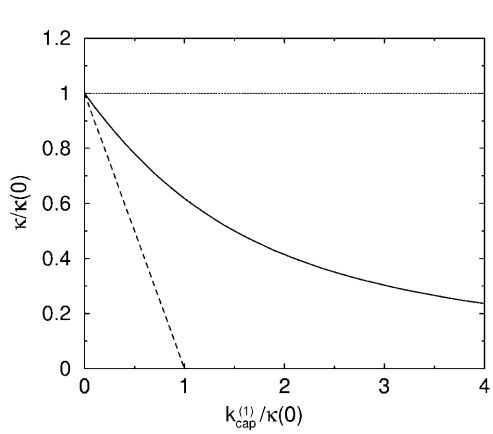

FIGURE 1 Calculated short-time autocatalytic growth rates κ for side-branching model (*solid line*), end-branching model (*dashed line*), and modified end-branching model in which capped filaments can branch (*dotted line*). $k_{\mathrm{cap}}^{(1)}$ is the barbed-end capping rate. $\kappa(0)$ is the value of κ at $k_{\mathrm{cap}}^{(1)} = 0$.

EXPERIMENTAL METHODS

CP purification

The plasmid for the expression of mouse CP $\alpha1$ and $\beta2$ subunits (cDNA accession numbers U16740 and U10407, $\alpha1$ and $\beta2$, respectively) was constructed by Dorothy Schafer in a pET-3d vector using the strategy described (Soeno et al., 1998) for chicken $\alpha1\beta1$ CP. Mouse $\alpha1\beta2$ CP was expressed and purified from BL21 Star (DE3) *Escherichia coli* as described (Palmgren et al., 2001). Purified CP was stored at −70°C in 10 mM TrisCl at pH 8.0, 40 mM KCl, 0.5 mM DTT, and 50% glycerol. Concentration of CP was determined using the extinction coefficient $\varepsilon_{280\mathrm{nm}} = 76,300\,\mathrm{M}^{-1}\,\mathrm{cm}^{-1}$.

Arp2/3 complex purification

Arp2/3 complex was purified from bovine calf thymus as described (Higgs et al., 1999) with minor modifications. Purified complex was stored at −70°C in 20 mM Tris at pH 7.5, 100 mM KCl, 1 mM EGTA, 2 mM $MgCl_2$, 0.1 mM ATP, 0.5 mM DTT, 1 mM NaN_3, and 50% glycerol. Concentration of Arp2/3 complex was determined using the extinction coefficient $\varepsilon_{280\mathrm{nm}} = 224,000\,\mathrm{M}^{-1}\,\mathrm{cm}^{-1}$ (Egile et al., 1999).

GST-VCA purification

The plasmid for the expression of the VCA domains from human N-WASp as a GST-fusion in the pGEX-4T1 vector, constructed as described (Egile et al., 1999), was a kind gift from Marie-France Carlier. GST-VCA was expressed in BL21 Star *E. coli* and purified using glutathione-agarose and standard protocols. GST-VCA was stored at −70°C in 50 mM Tris at pH 8.0, 150 mM NaCl, 0.5 mM EDTA, 0.5 mM DTT, 1 mM NaN_3, and 50% glycerol. Concentration of GST-VCA was determined using the extinction coefficient $\varepsilon_{280\mathrm{nm}} = 30,600\,\mathrm{M}^{-1}\,\mathrm{cm}^{-1}$.

Actin polymerization assays

Actin was purified from chicken-breast skeletal muscle as described (Spudich and Watt, 1971). Actin monomers were purified by gel-filtration on a Sephacryl S-300 column ($V_t \sim 530$ ml; 2.6 × 100 cm) equilibrated in ATP-G-buffer (10 mM Tris at pH 7.5, 0.2 mM ATP, 0.5 mM DTT, and 0.2 mM $CaCl_2$). Actin was labeled with pyrenyliodoacetamide (Molecular Probes, Eugene, OR) as described (Cooper et al., 1983). Actin polymerization was followed by monitoring the fluorescence of pyrene-actin for 1000 s, at 25°C (with a reading taken every s) on a PTI Quantmaster spectrofluorimeter (Photon Technology International, Santa Clara, CA), with excitation at 368 nm and emission at 386 nm. Actin was used at a final concentration of 2.0 μM (5% pyrene labeled), with final buffer conditions of 10 mM Tris at pH 7.5, 100 mM KCl, 2 mM $MgCl_2$, 0.2 mM ATP, 0.5 mM DTT, 0.2 mM $CaCl_2$, and 1 mM EGTA. The G-actin was primed before the initiation of polymerization. To an aliquot of Ca^{2+}-G-actin in ATP-G-buffer a 1/10th volume of 10 mM EGTA; 1 mM $MgCl_2$ was added and the mixture preincubated for 90 s, at 25°C, to allow exchange of the Ca^{2+} for Mg^{2+} on the actin. A 1/20th volume of 200 mM Tris at pH 7.5, 2M KCl, 40 mM $MgCl_2$, and 20 mM EGTA was then added to initiate polymerization. Arp2/3 complex, GST-VCA and CP were in 10 mM Tris at pH 7.5, 100 mM KCl, 2 mM $MgCl_2$, 0.2 mM ATP, 0.5 mM DTT, 0.2 mM $CaCl_2$, and 1 mM EGTA.

Spectrin-actin seeded (SAS) polymerization assays

Spectrin-actin seeds (SAS) were prepared from human erythrocytes as described (DiNubile et al., 1995). Capping protein was added to the actin mixture immediately after the priming incubation followed by the addition of the polymerization salt and finally by addition of 10 μl SAS. The solution was mixed by pipetting up and down twice. The reaction mixture was then transferred to the cuvette, and the pyrene fluorescence intensity measured.

Capping protein nucleation assays

Capping protein was added to the actin mixture immediately after the priming incubation and treated as before.

Activated Arp2/3 complex and CP polymerization assays

Arp2/3 complex (at 14.3 nM), GST-VCA (at 25 nM), and CP were added together to the actin mixture immediately after the priming incubation and treated as before. The delay between the addition of the all the reactants, mixing, and the commencement of fluorescence measurements was 12–15 s. The critical concentration of actin in the absence and presence of CP was measured as described (Cooper and Pollard, 1985).

Quantitative modeling methods

Our kinetic model treats filament growth, Arp2/3 complex-induced branching, barbed-end capping by CP, pointed-end capping by Arp2/3 complex, spontaneous nucleation of filaments, nucleation of new filaments by CP, and nucleation of new filaments by Arp2/3 complex. It can treat side branching, end branching, or both, by appropriate choice of parameters. We use parts of it to evaluate the input parameters for our branching simulations, and the whole model to perform the branching simulations. The parameters in the model are adjusted to minimize the mean-squared error in the fit to the data, using the Berkeley Madonna package, Ver. 8.01 (http://www.BerkeleyMadonna.com).

The rate equations are as follows:

$$\frac{d[F]}{dt} = k_{nuc}^{spont}([G]-G_c^B)^3 - (k_{cap}^{B,+}[CP] + k_{cap}^{P,+}[Arp2/3])[F] + k_{cap}^{B,-}[F^B] + k_{cap}^{P,-}[F^P] \quad (5)$$

$$\frac{d[F^B]}{dt} = k_{nuc}^{CP}[CP]([G]-G_c^P)^6 + k_{cap}^{B,+}[CP][F] + k_{cap}^{P,-}[F^{BP}] - (k_{cap}^{B,-} + k_{cap}^{P,+}[Arp2/3])[F^B] \quad (6)$$

$$\frac{d[F^P]}{dt} = \{k_{br}^{end}([F]+[F^P]) + k_{br}^{side}[P_{br}]\}[Arp2/3]([G]-G_c^B)^2 + k_{nuc}^{Arp2/3}[Arp2/3](G-G_c^B)^2 + k_{cap}^{P,+}[Arp2/3][F] + k_{cap}^{B,-}[F^{BP}] - (k_{cap}^{P,-} + k_{cap}^{B,+}[CP])[F^P] \quad (7)$$

$$\frac{d[F^{BP}]}{dt} = k_{cap}^{B,+}[CP][F^P] + k_{cap}^{P,+}[Arp2/3][F^B] - (k_{cap}^{B,-} + k_{cap}^{P,-})[F^{BP}] \quad (8)$$

$$\frac{d[G]}{dt} = -k_{gr}^{B,+}([G]-G_c^B)([F]+[F^P]) - k_{gr}^{P,+}([G]-G_c^P)([F]+[F^B]) - 2\{k_{br}^{end}([F]+[F^P]) + k_{br}^{side}[P_{br}]\}[Arp2/3]([G]-G_c^B)^2 - 3k_{nuc}^{spont}([G]-G_c^B)^3 - 6k_{nuc}^{CP}[CP]([G]-G_c^P)^6 - 2k_{nuc}^{Arp2/3}[Arp2/3]([G]-G_c^B)^2 \quad (9)$$

$$\frac{d[P_{br}]}{dt} = k_{gr}^{B,+}([G]-G_c^B)([F]+[F^P]) + k_{gr}^{P,+}([G]-G_c^P)([F]+[F^B]) - k_{age}[P_{br}] \quad (10)$$

$$\frac{d[CP]}{dt} = -k_{nuc}^{CP}[CP]([G]-G_c^P)^6 + k_{cap}^{B,-}([F^B]+[F^{BP}]) - k_{cap}^{B,+}[CP]([F]+[F^P]) \quad (11)$$

$$\frac{d[Arp2/3]}{dt} = -\{k_{br}^{end}([F]+[F^P]) + k_{br}^{side}[P_{br}]\}[Arp2/3]([G]-G_c^B)^2 - k_{nuc}^{Arp2/3}[Arp2/3]([G]-G_c^B)^2 + k_{cap}^{P,-}([F^P]+[F^{BP}]) - k_{cap}^{P,+}[Arp2/3]([F]+[F^B]). \quad (12)$$

In these equations, B and P denote barbed and pointed ends, respectively, and plus (+) and minus (−) denote on and off rates. $[F]$, $[F^B]$, $[F^P]$, and $[F^{BP}]$ are the concentrations of filaments that are uncapped, or capped at the barbed and/or pointed ends, $[G]$ is the free-monomer concentration, and G_c^B and G_c^P are the critical concentrations. P_{br} is the concentration of filament subunits that are capable of forming side branches (which is equal to the polymerized-actin concentration in simple side-branching models). In the rate constants, the subscript *gr* denotes growth, *cap* denotes capping, *nuc* denotes nucleation, *br* denotes branching, and *age* denotes aging. The rates k_{nuc}^{spont}, k_{nuc}^{CP}, and $k_{nuc}^{Arp2/3}$ are for spontaneous, CP-induced (pointed-end growth), and Arp2/3 complex-induced (barbed-end growth) nucleation, respectively. The branching rate constants, k_{br}^{end} and k_{br}^{side}, are given per filament and per subunit along a filament, respectively. Aging refers to the decrease of the ability of subunits to form branches on the side of a filament over time (Ichetovkin et al., 2002). The justification for our choice of powers of concentration in the branching and nucleation terms is given below.

Evaluation of input parameters for branching models

The parameter values were obtained by fits to the polymerization data, except for three values taken from the literature. The values are summarized in Table 1. For the growth-rate parameters, we use the literature values (Higgs et al., 1999; Pollard, 1986) $k_{gr}^{B,+} = 8.7\,\mu M^{-1}\,s^{-1}$ (for pH 7.5) and $k_{gr}^{P,+} = 1.3\,\mu M^{-1}\,s^{-1}$. There is no published value of the pointed-end uncapping rate $k_{cap}^{P,-}$ corresponding to Arp2/3 complex detachment. However, pointed-end uncapping should lead to branch detachment, so the branch detachment rate can provide an upper bound to the uncapping rate. Recent experiments (Weaver et al., 2001; Blanchoin et al., 2000) have measured the time course of branch detachment. We have fit the data of Weaver et al. (2001) for the number of branched filaments as a function of time with an exponential function. This yields a detachment rate constant of $0.0018\ s^{-1}$, which is also consistent with the data of Blanchoin et al. (2000). We use this value of $k_{cap}^{P,-}$, and also perform a parallel series of fits with $k_{cap}^{P,-} = 0$. As described under Methods, we measured the critical concentrations $G_c^B = 0.07\,\mu M$ for the barbed end and $G_c^P = 0.69\,\mu M$ for the pointed end.

To obtain the remaining input parameters, we used several models corresponding to subsets of Eqs. 5–12.

TABLE 1 Parameter values

Parameter	$k_{cap}^{P,-} = 0.0018\ s^{-1}$	$k_{cap}^{P,-} = 0$	Source
G_C^B	0.07 μM	0.07 μM	Present
G_C^P	0.69 μM	0.69 μM	Present
$k_{gr}^{B,+}$	8.7 $\mu M^{-1}\ s^{-1}$	8.7 $\mu M^{-1}\ s^{-1}$	(Higgs et al., 1999)
$k_{gr}^{P,+}$	1.3 $\mu M^{-1}\ s^{-1}$	1.3 $\mu M^{-1}\ s^{-1}$	(Pollard, 1986)
$k_{cap}^{B,+}$	8.0 $\mu M^{-1}\ s^{-1}$	8.0 $\mu M^{-1}\ s^{-1}$	Model I
$k_{cap}^{P,+}$	0.71 $\mu M^{-1}\ s^{-1}$	0.18 $\mu M^{-1}\ s^{-1}$	Model IV - end
	1.07 $\mu M^{-1}\ s^{-1}$	0.36 $\mu M^{-1}\ s^{-1}$	Model IV - side
	0.98 $\mu M^{-1}\ s^{-1}$	0.27 $\mu M^{-1}\ s^{-1}$	Model IV - end-plus-side
	0.80 $\mu M^{-1}\ s^{-1}$	0.33 $\mu M^{-1}\ s^{-1}$	Model V
$k_{cap}^{B,-}$	$4.2 \times 10^{-4}\ s^{-1}$	$4.2 \times 10^{-4}\ s^{-1}$	Model I
k_{nuc}^{spont}	$1.05 \times 10^{-9}\ \mu M^{-2}\ s^{-1}$	$1.05 \times 10^{-9}\ \mu M^{-2}\ s^{-1}$	Model II
k_{nuc}^{CP}	$2.9 \times 10^{-5}\ \mu M^{-6}\ s^{-1}$	$2.9 \times 10^{-5}\ \mu M^{-6}\ s^{-1}$	Model III
$k_{nuc}^{Arp2/3}$	$8.7 \times 10^{-5}\ \mu M^{-2}\ s^{-1}$	$1.19 \times 10^{-4}\ \mu M^{-2}\ s^{-1}$	Model IV - end
	$1.1 \times 10^{-5}\ \mu M^{-2}\ s^{-1}$	$6.8 \times 10^{-6}\ \mu M^{-2}\ s^{-1}$	Model IV - side
	$8.7 \times 10^{-6}\ \mu M^{-2}\ s^{-1}$	0	Model IV - end-plus-side
	0	0	Model V
k_{br}^{end}	0.29 $\mu M^{-3}\ s^{-1}$	0.158 $\mu M^{-3}\ s^{-1}$	Model IV - end
	0.082 $\mu M^{-3}\ s^{-1}$	0.43 $\mu M^{-3}\ s^{-1}$	Model IV - end-plus-side
k_{br}^{side}	$5.4 \times 10^{-4}\ \mu M^{-3}\ s^{-1}$	$6.0 \times 10^{-4}\ \mu M^{-3}\ s^{-1}$	Model IV - side
	$5.3 \times 10^{-4}\ \mu M^{-3}\ s^{-1}$	$4.9 \times 10^{-4}\ \mu M^{-3}\ s^{-1}$	Model IV - end-plus-side
	$1.44 \times 10^{-3}\ \mu M^{-3}\ s^{-1}$	$1.22 \times 10^{-3}\ \mu M^{-3}\ s^{-1}$	Model V
k_{age}	0.0087 s^{-1}	0.0059 s^{-1}	Model V

In rate constants, subscript *gr* denotes growth, *cap* denotes capping, *nuc* denotes nucleation, *br* denotes branching, and *age* denotes aging; superscripts *P* and *B* denote pointed and barbed ends, respectively. Pointed-end capping is by *Arp2/3* complex and barbed-end capping is by *CP*. Columns headed $k_{cap}^{P,-} = 0.0018\ s^{-1}$ and $k_{cap}^{P,-} = 0$ denote fits obtained with these values of $k_{cap}^{P,-}$.

Model I includes Eqs. 5–9, and 11, neglecting the k_{br}, k_{cap}^{P}, $k_{nuc}^{Arp2/3}$, and k_{nuc}^{CP} terms. It was used to evaluate $k_{cap}^{B,+}$ and $k_{cap}^{B,-}$ from the polymerization kinetics (progress curves) of a solution of spectrin-actin seeds (SAS) in 2 μM actin and varying concentrations of CP. The k_{nuc}^{CP} terms are ignored because of the very low concentrations of CP used in these experiments. The initial density of SAS ($[FP]$ at $t = 0$) was used as a fitting parameter, which gave a value of 0.11 nM. Fig. 2 shows that Model I gives a good fit to the data. The best-fit value of $k_{cap}^{B,+}$ is 7.99 $\mu M^{-1}\ s^{-1}$, consistent with the range of values observed previously (Schafer et al., 1996). We note that we used bacterially expressed CP, and previous studies used CP purified from tissue. In both cases, the $\beta 1$ and $\beta 2$ isoforms gave similar results. The value of $k_{cap}^{B,-}$ is $4.16 \times 10^{-4}\ s^{-1}$, also in line with the previous estimates.

Model II includes the k_{nuc}^{spont} term of Eq. 5, and the k_{gr} and k_{nuc}^{spont} terms of Eq. 9. It was used to obtain k_{nuc}^{spont} from the measured polymerization kinetics of a 2 μM actin solution. Fig. 3 (*lowest curve*, multiplied by a factor of 2 for visibility) shows that the fit, with $k_{nuc}^{spont} = 1.05 \times 10^{-9}\ \mu M^{-2}\ s^{-1}$, is quite accurate. This model is simpler than the multistep models (Frieden, 1983; Buzan and Frieden, 1996) generally used to study filament nucleation, but the quality of the fit indicates that it is sufficiently accurate to describe the limited range of times, and the single initial concentration, employed here.

Model III treats CP-induced filament nucleation using Eqs. 5, 6, 9, and 11, neglecting all k_{br} terms and terms involving [Arp2/3]. We obtained k_{nuc}^{CP} using this model, by measuring the polymerization kinetics of a solution of 2 μM actin in the presence of concentrations of CP varying from 0 to 25 nM. Fig. 3 shows that the polymerization is strongly accelerated by CP, indicating that at these concentrations, CP-induced nucleation dominates spontaneous nucleation. The fit, with $k_{nuc}^{CP} = 2.94 \times 10^{-5}\ \mu M^{-6}\ s^{-1}$, is excellent. Because the correct choice of power of concentration to use in Model III is not clear, we have tried other powers as well. Using a rate

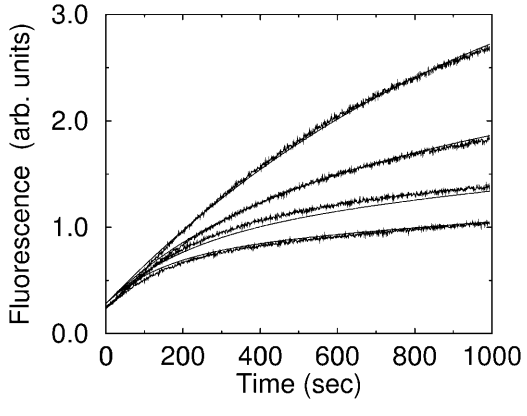

FIGURE 2 Effect of CP on polymerization of spectrin-actin seeds. [*CP*] increases from top to bottom: 0 nM, 0.25 nM, 0.5 nM, and 0.75 nM. Smooth curves, Model I.

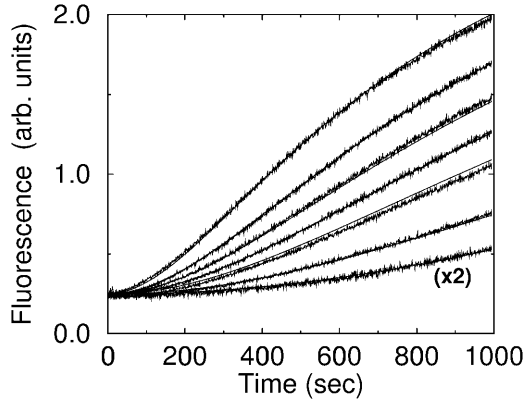

FIGURE 3 Spontaneous nucleation of actin filaments, and nucleation by CP. CP concentration increases from bottom to top: 0 nM, 2 nM, 5 nM, 7 nM, 10 nM, 15 nM, and 25 nM. Smooth curves, Model II (*bottom curve*, multiplied by a factor of 2 for visibility) and Model III (*remaining curves*).

proportional to $(G - G_c^B)^3$ instead of $(G - G_c^B)^6$ gives a fit that is somewhat worse but still quite acceptable. The sixth power may give a better fit by giving a combined description of multiple steps treated in more complete models (Cooper and Pollard, 1985).

Results for branching models

In our comparisons between different branching models, we use the parameters determined above where possible. However, because we cannot ascertain all of the parameters independently, we include parameters that are allowed to vary to optimize the fit. Figs. 4–7 show the polymerization kinetics of a solution of 2 μM actin, 14.3 nM Arp2/3 complex, 25nM GST-VCA, and CP concentrations ranging up to 25 nM. The CP slows the polymerization, changing the characteristic time over which the actin goes from mainly monomeric to mainly polymerized from approximately one hundred to several hundred seconds. The fitting errors (in arbitrary units, but consistent from model to model) obtained for several branching models are given in Table 2. In the curve fits given in Figs. 4–7, we use $k_{cap}^{P,-} = 0.0018\,s^{-1}$; the error values for $k_{cap}^{P,-} = 0$ are given in Table 2.

We use two models in our branching simulations:

Model IV treats branching polymerization in the absence of subunit aging effects. The rate equations include all of Eqs. 5–12, with $k_{age} = 0$. End branching is obtained by taking $k_{br}^{side} = 0$, and side branching by taking $k_{br}^{end} = 0$; an *end-plus-side* model is obtained by allowing both of these rates to be nonzero. The rate of formation of new branches should be proportional to the concentration of free, activated Arp2/3 complex, which we take to be proportional to the total concentration of free Arp2/3 complex. Provided that the timescale of the activation of Arp2/3 complex by GST-VCA is less than the characteristic time over which the actin polymerizes, this will be an accurate approximation. A value of 0.8 $\mu M^{-1}\ s^{-1}$ has been measured (Marchand et al., 2001) for the rate of WASp-VCA attachment to Arp2/3 complex, which would give a rate of 0.02 s^{-1} with our value of 25 nM for the GST-VCA concentration if we assume the same rate constant; in addition, an activation step with a rate constant of 0.034 s^{-1} has been found (Zalevsky et al., 2001). These rates are much faster than the characteristic rates for our Arp2/3 complex-induced polymerization curves shown below, with the exception of the $[CP] = 0$ curve. The power of 2 in the $(G - G_c^B)^2$ factor multiplying the k_{br} terms gives the best overall fit to the data, as discussed below.

In Fig. 4, the data are fit to the end-branching model. There are three fitting parameters: k_{nuc}^{Arp}, $k_{cap}^{P,+}$, and k_{br}^{end}. In the $[CP] = 0$ curve the data shows a pronounced overshoot in the polymerized fraction, which cannot be modeled within the constraints of the models used here. It is absent in the remaining curves, which have lower polymerization rates. For this reason, and because of the lag time for Arp2/3 complex activation discussed above, we give the $[CP] = 0$ curve zero fitting weight in most of our runs. However, we perform a few additional runs to establish whether this choice affects the relative quality of fit of the models. The end-branching model provides a poor description of the variation of the polymerization kinetics with $[CP]$. The general tendency of this model is to cut off polymerization too abruptly at large times. To make up for this tendency, the fit procedure adjusts $k_{nuc}^{Arp2/3}$ to a very high value, and this results in much too rapid polymerization at early times. When the value of $k_{nuc}^{Arp2/3}$ is limited to smaller values, the end-branching model gives much too low a polymerized fraction at large times.

We have also considered a variant of this model in which CP at filament ends does not prevent branch formation (see the *CP allow* results in Table 2). This gives a somewhat better fit than the conventional end-branching model, but much better fits are obtained with the side-branching models described below. Allowing for the possibility that capped filaments can branch at a rate less than uncapped ones results in a ''combined'' four-parameter model which, however, fits only marginally better than the *CP allow* model (see Table 2.)

The side-branching model gives a better description, as is seen in Fig. 5. The overall shape of the experimental data is well reproduced. The main deficiency of the model is that the curves for low $[CP]$ have too small a slope, whereas those at high $[CP]$ have too high a slope, and thus the effect of increasing $[CP]$ is somewhat underestimated. The error (Table 2) of this

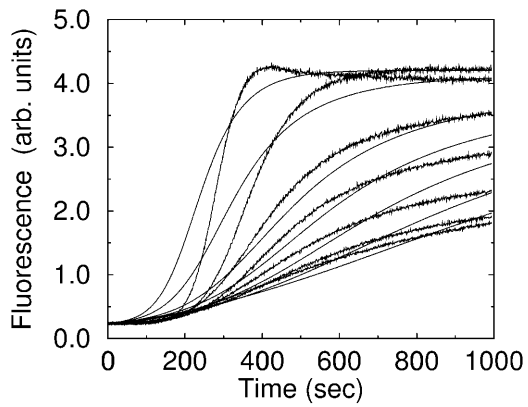

FIGURE 5 Side-branching model for Arp2/3 complex-induced polymerization of actin. Capping protein concentration increases from top to bottom: 0 nM, 2 nM, 5 nM, 7 nM, 10 nM, 15 nM, and 25 nM. Smooth curves, Model IV, with $k_{br}^{end} = 0$.

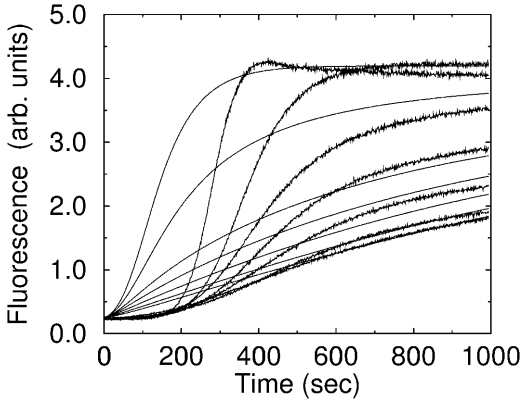

FIGURE 4 Effect of CP on Arp2/3 complex-induced polymerization of actin. Capping protein concentration increases from top to bottom: 0 nM, 2 nM, 5 nM, 7 nM, 10 nM, 15 nM, and 25 nM. Smooth curves, Model IV with $k_{br}^{side} = 0$.

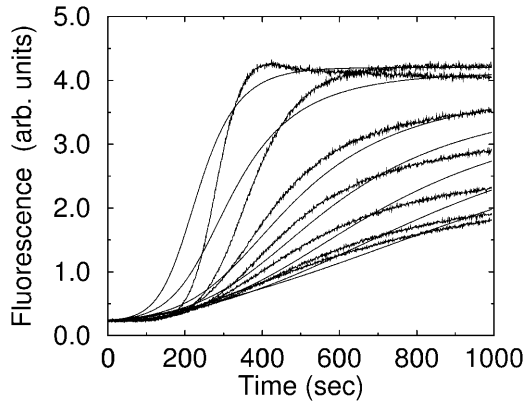

FIGURE 6 End-plus-side model for Arp2/3 complex-induced polymerization of actin. Capping protein concentration increases from top to bottom: 0 nM, 2 nM, 5 nM, 7 nM, 10 nM, 15 nM, and 25 nM. Smooth curves, Model IV.

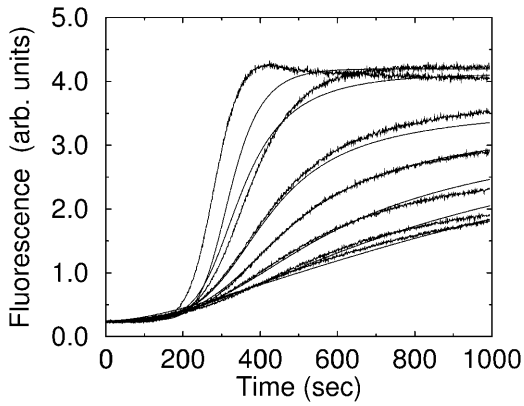

FIGURE 7 Aging model for Arp2/3 complex-induced polymerization of actin. Capping protein concentration increases from top to bottom: 0 nM, 2 nM, 5 nM, 7 nM, 10 nM, 15 nM, and 25 nM. Smooth curves, Model V.

model, for both values of $k_{cap}^{P,-}$, is less than half that of the end-branching model. To evaluate the reliability of the fit, we have performed several other runs. Keeping the $[CP] = 0$ curve in the fitting procedure gives results essentially identical to the previous ones. We have also varied the exponent m in the proportionality of the branching rate to $(G - G_c^B)^m$. As seen in Table 2, varying m in the range 1–3 results in variations of ~10 to 20% in the error. Although the $m = 3$ error for $k_{cap}^{P,-} = 0.0018\ s^{-1}$ is slightly less than that for $m = 2$, we use $m = 2$ in most of calculations. This allows us to compare the models on a roughly equal footing without including one more fitting parameter, since $m = 2$ gives close to the minimum error for all of the models with errors of 10 or below. Fig. 6 shows the fit for the end-plus-side model, with four fitting parameters. The error for $k_{cap}^{P,-} = 0.0018\ s^{-1}$ is only marginally reduced, but that for $k_{cap}^{P,-} = 0$ is reduced by ~25%.

Model V treats the aging model, in which branches form along filament sides, and the ability of subunits to form new branches ages at a rate k_{age}. It uses Eqs. 5–12, with $k_{br}^{end} = 0$. As Fig. 7 shows, it gives the best fit of any of the models treated. In Table 2, the errors are considerably smaller than those for the end-plus-side model. Since the aging model has the same number of adjustable parameters as the end-plus-side model (four), it appears to be a much better choice. In fact, the discrepancies between this model's predictions and the experimental data are smaller than the differences between this model and any of the other models. It is not clear what the aging process is. The value of k_{age}, 0.0059 s^{-1}–0.0087 s^{-1}, is much smaller than the ATP hydrolysis rate constant, 0.3 s^{-1} (Blanchoin and Pollard, 2002). It is closer to the phosphate release rate, which is in the range 0.002–0.003 s^{-1} (Melki et al., 1996; Blanchoin and Pollard, 1999). However, k_{age} exceeds these values by a factor of 2 to 4, suggesting that phosphate release is not the only factor governing aging. One possibility is that a partial reduction in subunits' ability to generate new branches occurs upon rapid hydrolysis, with a greater reduction coming with subsequent phosphate release. Disentangling these two contributions is probably beyond the resolution of the types of experiments described here. Examination of Table 1 shows that inclusion of aging effects increases the rate constant for side branching by a factor of 2 to 3. This is expected, since the number of branching-competent monomers is reduced by the aging effects, and the increased rate constant per monomer compensates for this reduction.

TABLE 2 Quality of fit

Model	$k_{cap}^{P,-} = 0.0018\ s^{-1}$	$k_{cap}^{P,-} = 0$	With $[CP] = 0$	N_{par}
IV				
End branching	22.8	24.6	33.8	3
(CP allow)	19.3	19.1		3
(Combined)	19.2	19.0		4
Side branching	9.8	8.2	12.7	3
$(([G] - G_c^B)^1)$	10.7	9.8		3
$(([G] - G_c^B)^3)$	9.7	8.4		3
End-plus-side	9.8	6.4	10.0	4
V				
Side branching	4.2	4.4	6.4	4
$(([G] - G_c^B)^1)$	4.8	4.8		4
$(([G] - G_c^B)^3)$	10.6	7.4		4

Errors given in arbitrary units, same in all models. Runs, in general, leave the $[CP] = 0$ curve out of the fitting procedure. The column labeled *With [CP] = 0* indicates the error obtained by minimizing with this curve, N_{par} is the number of fitting parameters.

Examination of the *With [CP] = 0* column in Table 2 shows that our conclusions are robust to inclusion of this curve in the fitting procedure. Side branching fits better than end branching, and Model V gives the best fit.

However, none of the models accurately describes the $[CP] = 0$ curve. As mentioned above, this curve has an overshoot in the polymerized fraction that is not obtained by any of our model variants. A similar overshoot was seen when light scattering was used in a control experiment without CP (data not shown), so the overshoot is not an artifact of the pyrene label. No actin polymerization theories to date have predicted this feature correctly, which may require inclusion of ATP hydrolysis, phosphate release, or annealing/severing of filaments. These processes can have a substantial effect on the critical concentration (Pantaloni et al., 1984).

We have not performed experiments for other actin or Arp2/3 complex concentrations. However, we have run simulations for some of the concentrations used by Pantaloni et al. (2000). The qualitative behavior of the simulations is consistent with their results, with the characteristic rate for polymerization increasing with the Arp2/3 complex concentration. Obtaining a quantitative fit to this data would involve revising several of the simulation parameters because of the different experimental conditions.

DISCUSSION

The analysis presented above has two main conclusions. First, if branching is restricted to a single type of model, side-branching models fit the experimental polymerization data better than end-branching models. Second, a model incorporating aging effects, in which the branching ability of subunits decays over time, gives significant improvements over end-plus-side models. Thus, most of the branching occurs along the sides of filaments, and newly formed portions of the filaments support a higher rate of branching.

These findings can help discriminate between several branching models that have been proposed previously. Support for end-branching models has been drawn (Pantaloni et al., 2000) from both electron-microscopy images of branched filaments and the polymerization kinetics in the presence of activated Arp2/3 complex. The electron-microscopy images showed a strong correlation between the lengths of mother and daughter filaments, suggesting dominance of end branching. The kinetic arguments favoring end branching were based on three types of experimental protocols. We have used our rate-equation methodology to model these results. Model V explains all three data sets, whereas Model IV explains the results for only two. The experiments were as follows:

Actin polymerization after addition of Arp2/3 complex at a delay time t_0 after the initiation of polymerization.

Measurements of the time $\Delta t_{1/2}$ after t_0 required to reach 50% polymerization suggested that $\Delta t_{1/2}$ decreases with t_0 but stabilizes at a value of t_0 at which the polymerized actin concentration $[P]$ is still increasing. Since the branch generation rate in side-branching models is proportional to $[P]$, this would appear to refute side-branching models. However, because the polymerization is autocatalytic, it has an exponential time dependence. Therefore the time required to reach a certain value of $[P]$ should depend only logarithmically on the initial value of $[P]$. Over a finite observation interval, it is difficult to distinguish a logarithmic variation from an approach to a limit. Our simulations for Model IV confirm the slow variation of $\Delta t_{1/2}$ with t_0. In the simulations for Model V, $\Delta t_{1/2}$ approaches a finite limit with increasing t_0, giving a somewhat better description of the experimental data than Model IV.

Actin polymerization in the presence of varying numbers of seed filaments, with the initial value of $[P]$ fixed. The polymerization rate increased with the number of seed filaments. In side-branching models, the filament generation rate should be mainly determined by $[P]$, leading to little variation with the number of seed filaments. Our simulations confirm this expectation, so that these experimental results cannot be explained by Model IV. However, in Model V, increasing the number of seed filaments increases the density of freshly polymerized actin, which enhances the branching rate. In our simulations, the polymerization thus is accelerated by the larger number of seed filaments. The effect is, however, significantly smaller than the experimental one.

Actin polymerization in the presence of a constant number of seed filaments, with lengths of 0.04 μm, 1 μm, or 2 μm. The polymerization rate was affected only slightly by the filament lengths. In side-branching models, the filament generation rate should be proportional to the filament lengths. However, under the experimental conditions that were used, already 50 s into the experiment (a time much shorter than the time courses used) a filament would elongate by $\sim$3 μm, masking the initial differences between the filament lengths. Our simulations of Models IV and V yield very small effects from the filament-length differences, consistent with the experimental data.We also note that the functional antagonism between Arp2/3 complex and capping proteins, derived by Pantaloni et al. (2000) from the dependence of the critical concentration on the Arp2/3 and capping-protein concentrations, is consistent with our side-branching models. In both Models IV and V the critical concentration increases from the barbed-end value toward the pointed-end value as $[CP]$ increases. The value of $[CP]$ required to substantially change the critical concentration increases with [Arp2/3].

Subsequently, several fluorescence-microscopy studies have provided real-time images of the branch formation process. In the study of Amann and Pollard (2001) filaments of rhodamine-labeled actin were attached to a substrate, and their growth and branching monitored. Branches clearly formed from sides in many cases. New branches were formed on the average 1.56 ± 1.42 μm from the barbed end of the mother filaments, and no preference was found for branch formation right at either end of the mother filament. However, a modest preference for branching in the barbed-end half of the mother filament was found. In a similar study (Ichetovkin et al., 2002), phalloidin-labeled filaments were used as seeds for the growth of rhodamine-actin filaments, and side branching was again found to dominate. An observed correlation between mother and daughter branch lengths, and an increased branching frequency along newly formed filaments, suggested a preference for branching near, but not at, the barbed end. Another study (Fujiwara et al., 2002) used TMR-5-MA labeled actin, with filament motion reduced by use of methylcellulose in the solution rather than attachment to a substrate. Side branching dominated, but 10% of the new branches were formed near the barbed end. Unlike the other two fluorescence studies, new branches formed preferentially near pointed ends. Our results here support the dominance of side branching, found in all of the real-time fluorescence studies. They are also consistent with the small enhancement of branching near the filaments' barbed ends, noted in Amann and Pollard (2001) and Ichetovkin et al. (2002).

Relevance of the present results for actin polymerization in cells

In cells, new branches are formed in the vicinity of the obstacle (plasma membrane or intracellular pathogen) against which the growing actin network exerts its force. If the maximum distance at which new branches form is d, and both end and side branching are present, then the ratio $N_{\text{side}}/N_{\text{end}}$ of the number of filaments formed by side branching to the number formed by end branching is $k^{(1)}_{\text{br,side}}d/k^{(1)}_{\text{br,end}}a$, where the k-values are effective first-order rate constants containing appropriate powers of concentration, and $a = 2.8$ nm is the step size per subunit along a filament (Holmes et al., 1990). If we assume the same concentration factors for side and end branching, then $N_{\text{side}}/N_{\text{end}} = k^{\text{side}}_{\text{br}}d/k^{\text{end}}_{\text{br}}a$. The value of d is not precisely known. However, an approximate upper bound for the width of the branching region is the spacing l_{br} between branches. If new branches formed much farther than l_{br} from the obstacle, then an increase in the network density going away from the obstacle would be observed in electron micrographs, and such an increase is not seen (Svitkina et al., 1997; Svitkina and Borisy, 1999). We therefore assume that $d \leq l_{\text{br}}$; l_{br} is roughly 15 subunit spacings (Svitkina and Borisy, 1999). Then, $N_{\text{side}}/N_{\text{end}} \leq 15k^{\text{side}}_{\text{br}}/k^{\text{end}}_{\text{br}}$. In the end-plus-side model (Table 1, using the set with smaller $k^{\text{end}}_{\text{br}}$),

$k_{br}^{side} = 5 \times 10^{-4}\,\mu M^{-3}\,s^{-1}$ and $k_{br}^{end} = 0.08\,\mu M^{-3}\,s^{-1}$, so $N_{side}/N_{end} \leq 0.09$; if $k_{br}^{side} = 1.4 \times 10^{-3}\,\mu M^{-3}\,s^{-1}$ is taken from the aging model, we obtain $N_{side}/N_{end} \leq 0.3$. Thus, even though most of the branches in the in vitro studies are formed along filament sides, the same rate parameters could lead to most filaments being formed at filament ends in the cellular environment. For side branching to be the dominant mechanism in the cellular environment, the ratio $k_{br}^{end}/k_{br}^{side}$ would need to be very low.

SUPPLEMENTARY MATERIAL

An online supplement to this article can be found by visiting BJ Online at http://www.biophysj.org.

We are grateful to Marie-France Carlier for supplying plasmids used in our GST-VCA purification protocol.

This research was supported by the National Institutes of Health under grant GM38542.

REFERENCES

Amann, K. J., and T. D. Pollard. 2001. Direct real-time observation of actin filament branching mediated by Arp2/3 complex using total internal reflection fluorescence microscopy. *Proc. Natl. Acad. Sci. USA.* 98:15009–15013.

Blanchoin, L., K. J. Amann, H. N. Higgs, J.-P. Marchand, D. A. Kaiser, and T. D. Pollard. 2000. Direct observation of dendritic actin filament networks nucleated by Arp2/3 complex and WASP/Scar proteins. *Nature.* 404:1007–1011.

Blanchoin, L., and T. D. Pollard. 1999. Mechanism of interaction of *Acanthamoeba* actophorin (ADF/cofilin) with actin filaments. *J. Biol. Chem.* 274:15538–15546.

Blanchoin, L., and T. D. Pollard. 2002. Hydrolysis of ATP by polymerized actin depends on the bound divalent cation but not profilin. *Biochemistry.* 41:597–602.

Buzan, J. M., and C. Frieden. 1996. Yeast actin: polymerization kinetic studies of wild type and a poorly polymerizing mutant. *Proc. Natl. Acad. Sci. USA.* 93:91–95.

Cooper, J. A., and T. D. Pollard. 1985. Effect of capping protein on the kinetics of actin polymerization. *Biochemistry.* 24:793–799.

Cooper, J. A., S. B. Walker, and T. D. Pollard. 1983. Pyrene actin: documentation of the validity of a sensitive assay for actin polymerization. *J. Muscle Res. Cell Motil.* 4:253–262.

DiNubile, M. J., L. Cassimeris, M. Joyce, and S. H. Zigmond. 1995. Actin filament barbed-end capping activity in neutrophil lysates—the role of capping protein-β(2). *Mol. Biol. Cell.* 6:1659–1671.

Egile, C., T. P. Loisel, V. Laurent, R. Li, D. Pantaloni, P. J. Sansonetti, and M.-F. Carlier. 1999. Activation of the Cdc42 effector N-WASp by the *Shigella flexneri* IcsA protein promotes actin nucleation by Arp2/3 complex and bacterial actin-based motility. *J. Cell Biol.* 146:1319–1332.

Frieden, C. 1983. Polymerization of actin: mechanism of the Mg^{2+}-induced process at pH 8 and 20°C. *Proc. Natl. Acad. Sci. USA.* 80:6513–6517.

Fujiwara, I., S. Suetsugu, S. Uemura, T. Takenawa, and S. Ishiwata. 2002. Visualization and force measurement of branching by Arp2/3 complex and N-WASP in actin filament. *Biochem. Biophys. Res. Commun.* 293:1550–1555.

Higgs, H. N., L. Blanchoin, and T. D. Pollard. 1999. Influence of the C terminus of Wiskott-Aldrich syndrome protein WASp and the Arp2/3 complex on actin polymerization. *Biochemistry.* 38:15212–15222.

Higgs, H. N., and T. D. Pollard. 2001. Regulation of actin filament formation through Arp2/3 complex. *Annu. Rev. Biochem.* 70:649–676.

Holmes, K. C., D. Popp, W. Gebhard, and W. Kabsch. 1990. Atomic model of the actin filament. *Nature.* 347:44–49.

Ichetovkin, I., W. Grant, and J. Condeelis. 2002. Cofilin produces newly polymerized actin filaments that are preferred for dendritic nucleation by the Arp2/3 complex. *Curr. Biol.* 12:79–84.

Marchand, J.-B., D. A. Kaiser, T. D. Pollard, and H. N. Higgs. 2001. Interaction of WASp/Scar proteins with actin and vertebrate Arp2/3 complex. *Nat. Cell Biol.* 3:76–82.

Machesky, L. M., D. M. Mullins, H. N. Higgs, D. A. Kaiser, L. Blanchoin, R. C. May, M. E. Hall, and T. D. Pollard. 1999. Scar, a WASp-related protein, activates nucleation of actin filaments by the Arp2/3 complex. *Proc. Natl. Acad. Sci. USA.* 96:3739–3744.

Melki, R., S. Fievez, and M.-F. Carlier. 1996. Continuous monitoring of P_i release following nucleotide hydrolysis in actin or tubulin assembly using 2-amine-6-mercapto-7-methylpurine ribonucleoside and purine-nucleoside phosphorylase as an enzyme-linked assay. *Biochemistry.* 35:12038–12045.

Mullins, R. D., J. A. Heuser, and T. D. Pollard. 1998. The interaction of Arp2/3 complex with actin: nucleation, high-affinity pointed end capping, and formation of branching networks of filaments. *Proc. Natl. Acad. Sci. USA.* 95:6181–6186.

Palmgren, S., P. J. Ojala, M. A. Wear, J. A. Cooper, and P. Lappalainen. 2001. Interactions with PIP2, ADP-actin monomers, and capping protein regulate the activity and localization of yeast twinfilin. *J. Cell Biol.* 155:251–260.

Pantaloni, D., M.-F. Carlier, M. Coué, A. A. Lal, S. L. Brenner, and E. D. Korn. 1984. The critical concentration of actin in the presence of ATP increases with the number concentration of filaments and approaches the critical concentration of actin·ADP. *J. Biol. Chem.* 259:6274–6283.

Pantaloni, D., R. Boujemaa, D. Didry, P. Gounon, and M.-F. Carlier. 2000. The Arp2/3 complex branches filament barbed ends: functional antagonism with capping proteins. *Nat. Cell Biol.* 2:385–391.

Pollard, T. 1986. Rate constants for the reactions of ATP- and ADP-actin with the ends of actin filaments. *J. Cell Biol.* 103:2747–2754.

Pollard, T. D., L. Blanchoin, and R. D. Mullins. 2000. Molecular mechanisms controlling actin filament dynamics in nonmuscle cells. *Annu. Rev. Biophys. Biomol. Struct.* 29:545–576.

Robinson, R. C., K. Turbedsky, D. A. Kaiser, J.-B. Marchand, H. N. Higgs, S. Choe, and T. D. Pollard. 2001. Crystal structure of Arp2/3 complex. *Science.* 294:1679–1684.

Schafer, D. A., P. B. Jennings, and J. A. Cooper. 1996. Dynamics of capping protein and actin assembly in vitro: uncapping barbed ends by polyphosphoinositides. *J. Cell Biol.* 135:169–179.

Soeno, Y., H. Abe, S. Kimura, K. Maruyama, and T. Obinata. 1998. Generation of functional β-actinin (CapZ) in an *E. coli* expression system. *J. Muscle Res. Cell Motil.* 19:639–646.

Spudich, J. A., and S. Watt. 1971. The regulation of rabbit skeletal muscle contraction. *J. Biol. Chem.* 246:4866–4871.

Svitkina, T. M., and G. G. Borisy. 1999. Arp2/3 complex and actin depolymerizing factor/cofilin in dendritic organization and treadmilling of actin filament array in lamellipodia. *J. Cell Biol.* 145:1009–1026.

Svitkina, T. M., A. B. Verkhovsky, K. M. McQuade, and G. G. Borisy. 1997. Analysis of the actin-myosin II system in fish epidermal keratocytes: mechanism of cell body translocation. *J. Cell Biol.* 139:397–415.

Volkmann, N., K. J. Amann, C. E. Stoilova-McPhie, D. C. Winter, L. Hazelwood, J. E. Heuser, R. Li, T. D. Pollard, and D. Hanein. 2001. Structure of Arp2/3 complex in its activated state and in actin filament branch junctions. *Science.* 293:2456–2459.

Weaver, A. M., A. V. Karginov, A. W. Kinley, S. A. Weed, Y. Li, J. T. Parsons, and J. A. Cooper. 2001. Cortactin promotes and stabilizes Arp2/3-induced actin filament network formation. *Curr. Biol.* 11:370–374.

Zalevsky, J., L. Lempert, H. Kranitz, and R. D. Mullins. 2001. Different WASP family proteins stimulate different Arp2/3 complex-dependent actin-nucleating activities. *Curr. Biol.* 11:1903–1913.